Polymer 51 (2010) 4907–4915

Contents lists available at ScienceDirect

Polymer

journal homepage: www.elsevier.com/locate/polymer

Effect of organoclay structure and mixing protocol on the toughening of amorphous polyamide/elastomer blends

Youngjae Yoo [a], Rajkiran R. Tiwari [a], Young-Tai Yoo [b], Donald R. Paul [a,*]

[a] Department of Chemical Engineering and Texas Materials Institute, The University of Texas at Austin, Austin, TX 78712, United States
[b] Department of Materials Chemistry and Engineering, Konkuk University, Seoul 143-701, Republic of Korea

ARTICLE INFO

Article history:
Received 28 June 2010
Accepted 15 August 2010
Available online 21 August 2010

Keywords:
Amorphous polyamide
Elastomer
Blend nanocomposites

ABSTRACT

An amorphous polyamide (a-PA) was blended with an ethylene-1-octene (EOR) elastomer with organoclays present to control the elastomer particle size. Four different organoclays, $M_3(HT)_1$, $M_2(HT)_2$, $M_1H_1(HT)_2$, and $(HE)_2M_1T_1$ and two different mixing protocols were used to investigate the effect of the organoclay structure and mixing protocol on the morphology and properties of the resulting blends. Wide angle X-ray scattering, transmission electron microscopy, and stress-strain behavior were used to evaluate the degree of exfoliation of the organoclays and the morphology of the elastomer particles for these blends. A detailed particle analysis was made to provide a quantitative assessment of elastomer particle size. The size and shape of the elastomer particles were dramatically affected by the amount of organoclay but the organoclay type and the mixing protocol led to slight differences. Broadly speaking, most of the MMT platelets are well exfoliated in the a-PA phase, but some locate at the interface and tend to envelop the EOR phase. The mechanical properties were not significantly affected by the organoclay type or the mixing protocol. While the organoclays reduced the EOR particles to size range where toughness might be expected, all blends proved to be brittle. A clear trade-off was observed between the Izod impact strength and tensile modulus for these blends containing organoclays.

1. Introduction

For some time, our laboratory has explored the structure and properties of blends of elastomers with various polymers including polyamides, both crystalline and amorphous, and polyolefins containing organoclays [1–6]. Recently, blends of an amorphous polyamide, and an unmaleated ethylene-1-octene (EOR) elastomer containing various levels of organoclay were prepared to explore the possibility of enhancing toughness by tailoring the elastomer particle size via the effect the organoclay has on dispersed phase particle coalescence [6]. The resulting morphology changes and the toughening response were compared with the more conventional approach of blending this polyamide with a maleated version of this elastomer (EOR-g-MA) and with a reinforced version containing organoclays. It was demonstrated that addition of organoclay to such blends can be an effective way for reducing elastomer particle size and enhancing stiffness; however, toughness was not improved even though the reduction in elastomer particle size by the organoclay was comparable to that produced by grafting reactions between the amine chain ends and maleic anhydride units which does lead to supertough blends. The previous result was based on only one compounding procedure and a specific organoclay structure inspired from works done earlier [7–9]. Here, we explore similar blends using other types of organoclay and two mixing protocols.

Numerous other reports have shown that organoclay particles can dramatically reduce the size of the dispersed phase in a polymer blend [1,10–21]. Hong et al. [14]. observed that the addition of a small amount of organoclay decreased the size of the dispersed phase of immiscible PBT/PE polymer blends. Ray et al. [16]. investigated the role of organoclay as a compatibilizer for immiscible PS/PP blends. This study demonstrated that the organoclays located at the interface between the two polymers, reduced particle size, and apparently improved the mechanical properties. Also, Khatua et al. [15]. observed a significant decrease of the dispersed EPR phase of PA6/ethylene-propylene copolymer (EPR) blends with the addition of small amounts of organoclay. Similar observations were made for PA6/LLDPE blends [21]. This change may result from a “barrier” effect that limits the coalescence of the dispersed phases [15]. The effect of the change in viscosity ratio is also important [12,19,21].

* Corresponding author. Tel.: +1 512 471 5392; fax: +1 512 471 0542.
E-mail address: drp@che.utexas.edu (D.R. Paul).

0032-3861/$ – see front matter © 2010 Elsevier Ltd. All rights reserved.
doi:10.1016/j.polymer.2010.08.036

Table 1
Materials used in this study.

Material (designation in this paper)	Commercial designation	Specifications	Supplier
Polymer			
a-PA[a]	Zytel® 330	[COOH]/[NH2] = 4.5[b], T_g = 127 °C $\overline{M}_n$ = 14000[c], $\overline{M}_w$ = 50000[c]	Du Pont
EOR	Exact® 8201	28 wt% Octene MFR: ~22 g/10 min density = 0.884 g/cc	ExxonMobil
Organoclays[d]			
$M_3(HT)_1$	*Experimental*: Trimethyl hydrogenated-tallow ammonium montmorillonite	Organic loading = 95 mequiv/100 g clay Organic content = 29.6 wt % d_{001} spacing = 18.0 Å[e]	Southern Clay Products
$M_2(HT)_2$	*Cloisite® 20A*: Dimethyl bis(hydrogenated-tallow) ammonium montmorillonite	Organic loading = 95 mequiv/100 g clay Organic content = 39.6 wt % d_{001} spacing = 25.5 Å[e]	Southern Clay Products
$M_1H_1(HT)_2$	*Cloisite® 93A*: Methyl bis(hydrogenated-tallow) ammonium montmorillonite	Organic loading = 95 mequiv/100 g clay Organic content = 38.4 wt % d_{001} spacing = 23.3 Å[e]	Southern Clay Products
$(HE)_2M_1T_1$	*Cloisite® 30B*: Bis(2-hydroxy-ethyl)methyl tallow ammonium montmorillonite	Organic loading = 90 mequiv/100 g clay Organic content = 31.5 wt % d_{001} spacing = 17.7 Å[e]	Southern Clay Products

[a] 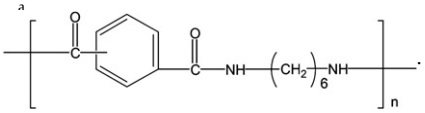

[b] Data from Ref. [50].
[c] Data from Ref. [51].
[d] The selected organoclay is designated as $M_2(HT)_2$ in this study, where M = methyl, T = tallow, HT = hydrogenated-tallow, and HE = 2-hydroxy-ethyl. Tallow is a natural product composed predominantly (63%) of saturated and unsaturated C_{18} chains. HT is the saturated form yet still contains a small fraction of double bonds.
[e] The basal spacing corresponds to the characteristic Bragg reflection peak d_{001} obtained from a powder WAXS scan of the organoclay.

Wang et al. [20]. proposed that parts of the polymer chains located outside the gallery of the clay serve as a compatibilizer. Dharaiya et al. [10]. explained that the decreased size of the dispersed phase of PP/PA blends can be attributed primarily to generation of thinner fibrils and subsequent breakup into smaller droplets in the presence of organoclays. Lee et al. [1]. described the "barrier" effect caused by the presence of clay particles and their influence on elastomer particle elongation during the injection molding process. However, increased domain size by organoclay addition has also been reported for some reactive blend systems [2,22,23].

This work complements recent efforts to determine the effects of organoclay structure and mixing protocols on the structure and properties of polymer blend nanocomposites. Lee et al. [24]. compared the effect of pristine montmorillonite (MMT) and two organoclays, Cloisite® 15A and Cloisite® 25A, and also varied the number of extrusion steps. They reported that, with multiple extrusion steps, the poly(methyl methacrylate) (PMMA) domain size became larger for blends of PMMA/poly(styrene-*co*-acrylonitrile) (SAN) containing pristine MMT while those with organoclays showed less growth in PMMA domain size. Vo et al. [18]. compared the effects oftwo organoclays, Cloisite® 30B and Cloisite® 20A, and simultaneous and sequential extrusions on poly(vinylidene fluoride) (PVDF)/nylon 6 blends. They demonstrated that blends containing Cloisite® 30B prepared by simultaneous extrusion had good dispersion of organoclay and reduced PVDF domain size and exhibited the best mechanical properties. The majority of organoclay dispersed in the nylon 6 matrix and some of the organoclay were observed at the PVDF/nylon 6 interface. Kelnar et al. [25]. showed that high levels of delamination of clay in the nylon 6 matrix and balanced mechanical behavior of nylon 6/EPR nanocomposites were achieved when combining two differently modified clays, Cloisite® 15A and Cloisite® 30B, where the clay with less polar treatment, Cloisite® 15A, was preblended with EPR. Dasari et al. [26]. reported that blending nylon 66 with organoclay, Cloisite® 30B, followed by mixing with SEBS-*g*-MA is the preferred blending sequence to maximize the notched impact strength. Similar results for nylon 6/ethylene-polypropylene-diene copolymer (EPDM) nanocomposites were reported by García-López et al [27]. On the other hand, Ha et al. [28]. observed similar morphology and mechanical properties for polyolefin ternary blends regardless of the mixing sequence. Wang et al. [29]. found that blending sequence had less influence on the mechanical properties and a one step blending sequence was selected as the simplest way to prepare PA6/EPDM-*g*-MA/organoclay ternary nanocomposites.

As an extension of our previous work [6], the purpose here is to explore and compare in some detail the toughening response of blends of a commercial amorphous polyamide, designated here as a-PA, with unmaleated EOR containing various organoclays prepared by two different mixing protocols. The effects of elastomer content and elastomer particle size on Izod impact strength and the ductile–brittle transition temperature are discussed. A detailed particle analysis for elastomer phases is presented and used to understand the mechanical properties of these blends. An additional objective of this work is to find the preferred organoclay structure and processing conditions for balanced mechanical properties and morphology of this blend.

2. Experimental section

Table 1 summarizes the materials used in this study. The amorphous polyamide, Zytel® 330, designated here as a-PA, was supplied by DuPont. The ethylene-1-octene copolymer, designated as EOR, was supplied by ExxonMobil. These materials have been used extensively in previous investigations in our laboratory; further information about these materials is given elsewhere [6,9,30–32]. Four kinds of organoclays were obtained from Southern Clay Products; these were formed by cation exchange reaction between Na^+ MMT and the surfactants shown in Fig. 1. These organoclays were chosen to determine the effect of the number of long alkyl tails, $M_3(HT)_1$ vs. $M_2(HT)_2$, type of amine, $M_1H_1(HT)_2$ vs. $M_2(HT)_2$, and the effect of hydroxyl ethyl functional groups, $(HE)_2M_1T_1$ vs. $M_3(HT)_1$.

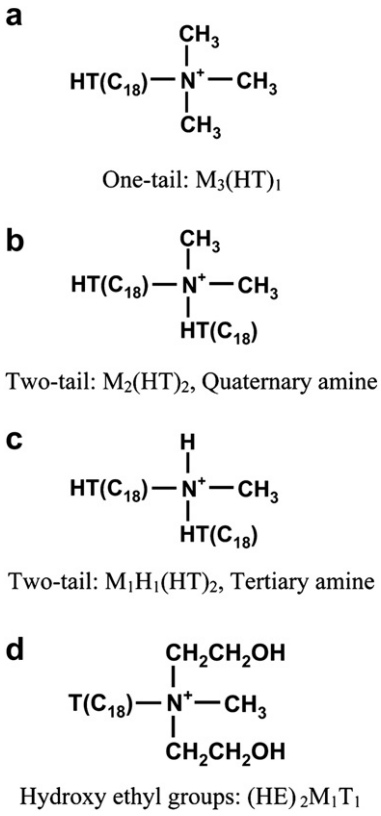

Fig. 1. Molecular structures used to organically modify sodium montmorillonite by ion exchange. The symbols M: methyl, T: tallow, HT: hydrogenated-tallow, and HE: 2-hydroxy-ethyl designate the substituents on the nitrogen.

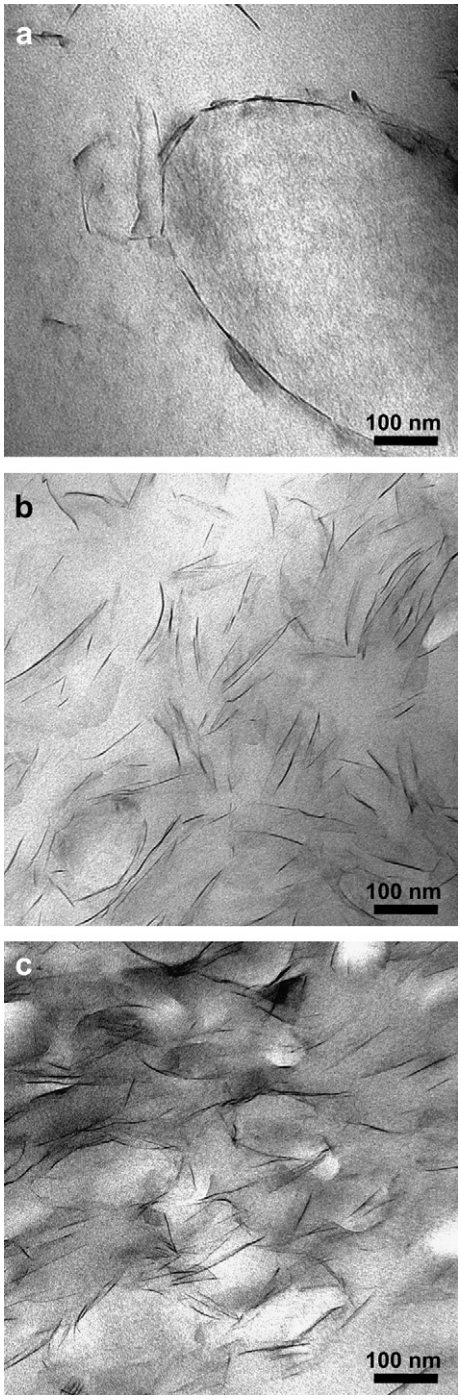

Fig. 2. Representative TEM micrographs of a-PA/EOR (80/20) blends prepared with the following mixing protocol and organoclay; (a) Protocol 1, 0.5 wt% $M_2(HT)_2$, (b) Protocol 2, 3.0 wt% $M_1H_1(HT)_2$, and (c) Protocol 2, 3.0 wt% $M_2(HT)_2$.

Prior to melt processing, a-PA was dried for a minimum of 24 h in a vacuum oven at 80 °C while the organoclay and EOR were used as-received. The a-PA/EOR blends containing organoclay were prepared using a Haake co-rotating, intermeshing twin-screw extruder (diameter = 30.5 mm, L/D = 10) operating at a barrel temperature of 240 °C, a feed rate of ~1 kg/h, and screw speed of 280 rpm. In order to study the effect of mixing protocols on the morphology and properties of the resulting nanocomposites, two different mixing protocols were adopted here: Protocol 1 involved a premix of a-PA and EOR with organoclay that was subsequently blended with more a-PA later. This sequence can be represented as [(a-PA (20 wt%) + EOR (20 wt%) + organoclay)+ a-PA (60 wt%)]. In protocol 2, a-PA was compounded with the organoclay first and then the a-PA/organoclay nanocomposite was blended with EOR later. This sequence can be represented as [(a-PA (80 wt %) + organoclay) + EOR (20 wt%)]. These procedures have been described more fully elsewhere [33]. For comparison, the a-PA/EOR blend without the organoclay was also prepared and passed through the extruder twice in order to have the same thermal and shear history as nanocomposites prepared here. Nanocomposite pellets were injection molded to prepare standard 3.18 mm thick tensile (ASTM D638) and Izod bars (ASTM D256) with an Arburg All-rounder 305-210-700 injection molding machine using a barrel temperature of 240 °C, mold temperature of 80 °C, injection pressure of 70 bar and a holding pressure of 35 bar. After molding, the samples were immediately sealed in a polyethylene bag and placed in a vacuum desiccator for a minimum of 24 h prior to testing. In this work, the a-PA/EOR weight ratio was fixed at 80/20. A total elastomer phase concentration of 20 wt% has been used extensively in several prior works and reflects the range of commercial rubber-modified polyamides since it is known to provide a reasonable balance of impact properties versus stiffness.

Morphology was determined by a JEOL 2010F transmission electron microscope (TEM) using ultra-thin sections of approximately 50 nm thickness cryogenically microtomed with a diamond knife using an RMC PowerTome XL microtome. The microtoming process has been fully described elsewhere [6,34,35]. A 2% aqueous solution of phosphotungstic acid (PTA) was used to stain the polyamide phase. Elastomer particle sizes were determined from

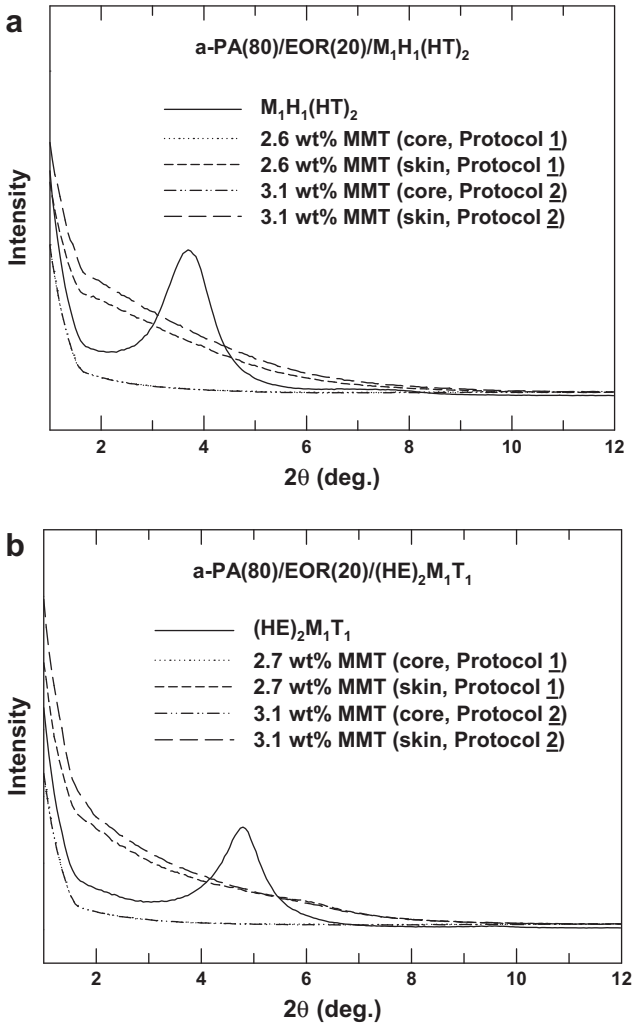

Fig. 3. Skin and core effects on WAXS scans of pristine organoclay and a-PA/elastomer (80/20) blends based on (a) $M_1H_1(HT)_2$, and (b) $(HE)_2M_1T_1$.

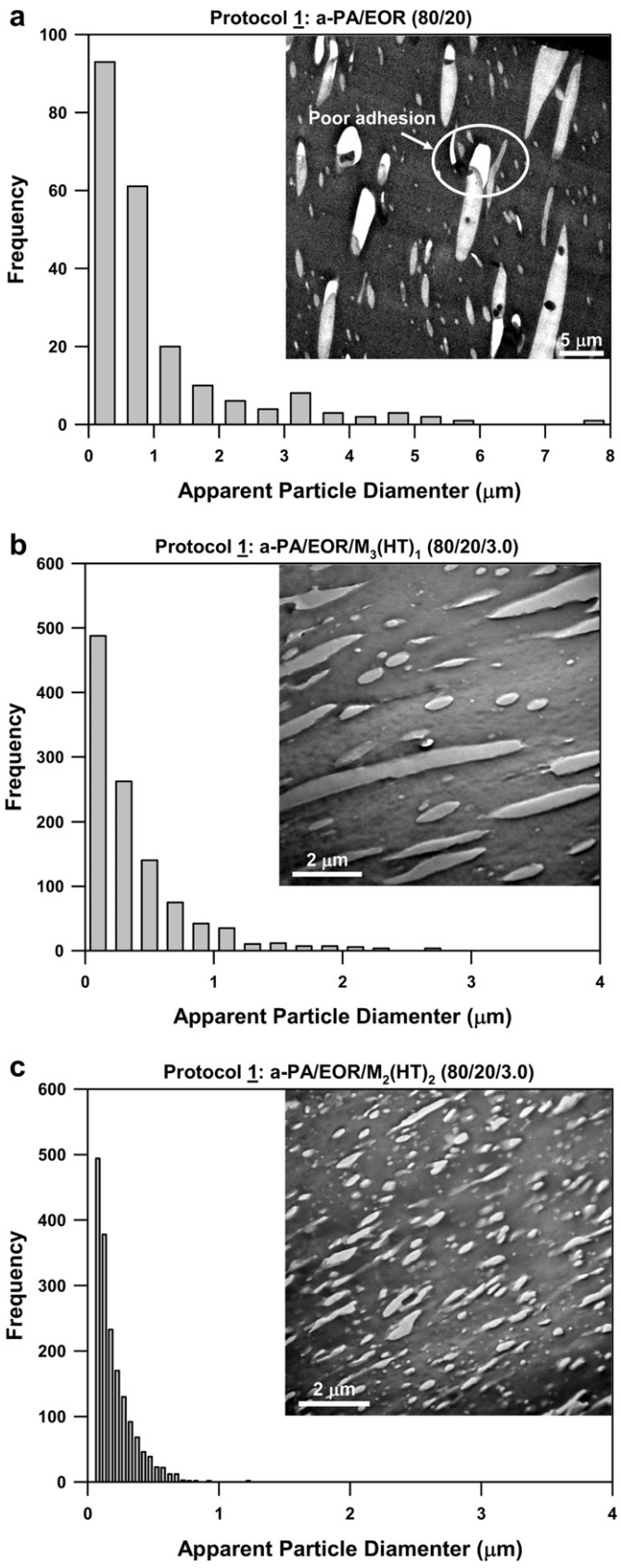

Fig. 4. TEM micrographs and histograms of apparent elastomer particle sizes obtained by analyzing TEM images of a-PA/EOR (80/20) blends prepared by protocol 1 with/without organoclay: (a) 0 wt% organoclay, (b) 3wt% $M_3(HT)_1$, and (c) 3wt% $M_2(HT)_2$.

TEM micrographs using a semi-automatic digital image analysis technique based on the NIH ImageJ software as described previously [6,30,32]. The calculation of average elastomer particle size has been described previously [6].

Wide angle X-ray scattering (WAXS) was performed using a Scintag XDS 2000 diffractometer in the reflection mode, using an incident X-ray wavelength of 0.154 nm at a scan rate of 1.0 deg/min. The four corresponding organoclays used in this work, i.e., $M_3(HT)_1$, $M_2(HT)_2$, $M_1H_1(HT)_2$ and $(HE)_2M_1T_1$, were scanned in the form of powder while injection molded samples of nanocomposites formed from them were also scanned such that the beam probed the skin of an Izod bar perpendicular to the FD. Additionally, the skin of the bar was removed by an automated milling machine prior to the WAXS scans in order to obtain information about the morphology in the core of the bar as explained elsewhere [6,9,36].

Tensile tests were performed according to ASTM D638 using an Instron model 1137 testing machine upgraded for computerized data acquisition. Values of the tensile modulus were determined using an extensometer. Modulus and yield strength data were determined at a crosshead rate of 0.51 cm/min. Izod impact tests were conducted using a TMI Impact tester (model 43-02) equipped with an insulated chamber for heating and cooling so that the samples could be tested at a variety of temperatures. The testing procedures are given elsewhere [37]. Values from the far and gate

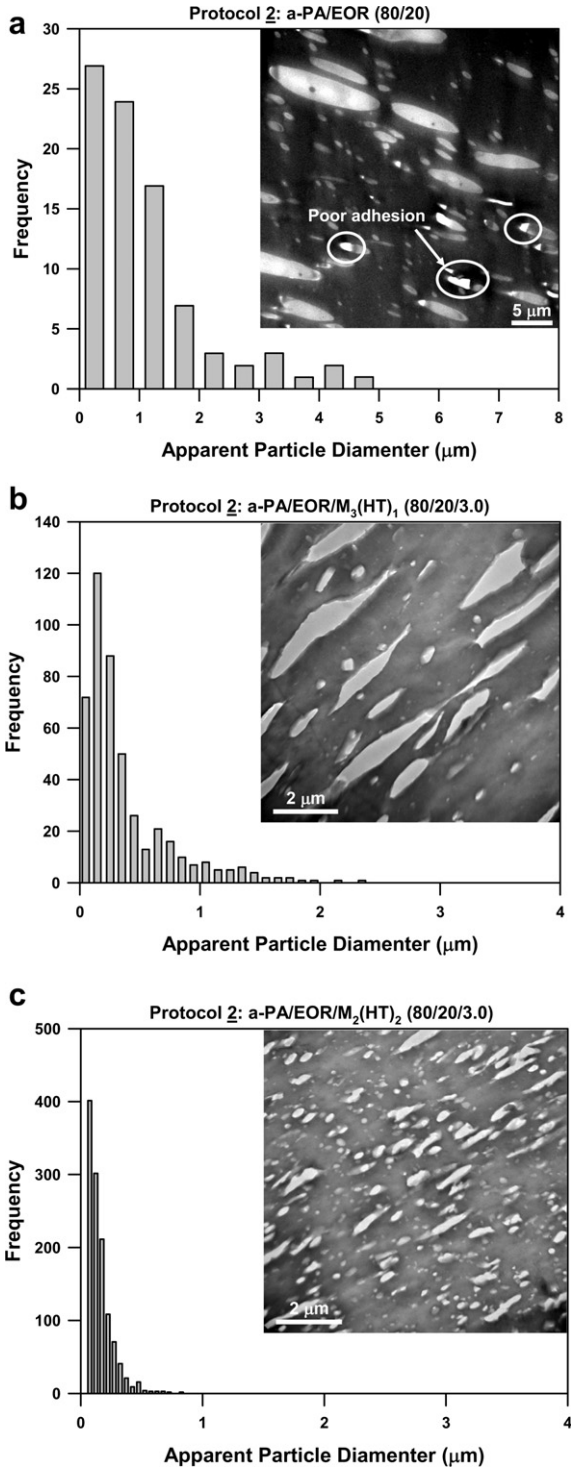

Fig. 5. TEM micrographs and histograms of apparent elastomer particle sizes obtained by analyzing TEM images of a-PA/EOR (80/20) blends prepared by protocol 2 method with/without organoclay: (a) 0 wt% organoclay, (b) 3wt% $M_3(HT)_1$, and (c) 3wt% $M_2(HT)_2$.

ends of injection molded samples were averaged together since the difference between the two is relatively small. The tested samples failed in three modes: a hinged break near the ductile–brittle transition temperature, a complete break below the ductile–brittle transition temperature and a mixed mode in the transition region where specimens of the same composition showed either a hinged or a complete break.

The data below are reported in terms of weight percent montmorillonite, wt% MMT, in the composite rather than the amount of organoclay, since this allows more meaningful comparisons among the different organoclays. The amount of MMT in the nanocomposites was determined by placing pre-dried extruded pellets in a furnace at 900 °C for 45 min and weighing the remaining MMT ash correcting for loss of structural water during incineration [7,38–42].

3. Morphology

TEM is an effective technique to qualitatively and quantitatively characterize the elastomer morphology as well as organoclay dispersion in a-PA/EOR blend. Fig. 2 shows representative TEM micrographs for nanocomposites with different organoclay structures and different mixing protocols. All micrographs were taken from the plane defined by the flow direction (FD) and the normal direction (ND) of the molded bar. Fig. 2(a) shows, as reported previously [6], that the organoclay is located in the a-PA phase or interface and not in the EOR phase for a nanocomposite based on $M_2(HT)_2$ containing 0.5 wt% MMT prepared by protocol 1. Interestingly, some of the organoclay tends to envelop the EOR phase as a single layer while the elastomer particles tend to maintain their original ellipsoidal shape. Fig. 2(b) and (c) show the morphology of blends prepared by protocol 2 with $M_1H_1(HT)_2$ and $M_2(HT)_2$ containing 3.1 wt% MMT. Similarly, clay tactoids are seen in the interface and in the a-PA phase. Previously [9], we explored the effect of the organoclay structure on the extent of exfoliation and properties of the nanocomposites based on a-PA without any elastomer. We reported that nanocomposites based on the organoclays with one alkyl tail, $M_3(HT)_1$, and hydroxyl ethyl groups, $(HE)_2M_1T_1$, gave well exfoliated structures and high matrix reinforcement while nanocomposites from two-tailed organoclay, $M_2(HT)_2$, contain a considerable concentration of unexfoliated tactoids. Interestingly, the organoclays in these blends show excellent exfoliation in the a-PA phase irrespective of the organoclay while some locates in the a-PA/EOR interface and tends to envelop the EOR phase. From this, it can be inferred that the organoclay preferentially locates at the interface for these blends. In this a-PA/EOR blend, elastomer particles are stabilized against coalescence by MMT platelets adsorbed at their interface. The effects are analogous to those in particle-stabilized water-oil emulsion, commonly described as 'Pickering' emulsions [43,44]. More intensive mixing from double extrusion and increased residence time contribute to exfoliation of MMT in the a-PA phase irrespective of the organoclay structure [45]. It is noted that the elastomer particles seem to affect the alignment of the MMT platelets in the immediate vicinity.

WAXS is a well-known technique for characterizing the state of organoclays in nanocomposites. Fig. 3 shows representative WAXS scans for $M_1H_1(HT)_2$ and $(HE)_2M_1T_1$ and their nanocomposites. To compare the structure between the skin and the core according to the two different mixing protocols, some specimens were precision milled to half depth of the original bar thickness. The scans from the core portion of injection molded specimens do not show a characteristic X-ray diffraction peak regardless of the organoclay or the mixing protocol. WAXS scans from the skin portion of these nanocomposites, on the other hand, have small diffraction peaks in some cases. Nanocomposites based on $(HE)_2M_1T_1$ have characteristic peaks at approximately $2\theta = 6–7°$ and $2–3°$ as shown in Fig. 3 (b), indicating the presence a population of intercalated tactoids. This means that some distinct structural differences exist between the skin and core of injection molded specimens of nanocomposites. This is not a result of differences in exfoliation levels from the skin to the core but the fact that the MMT particles are more oriented in the skin than the core as suggested by Lee et al.

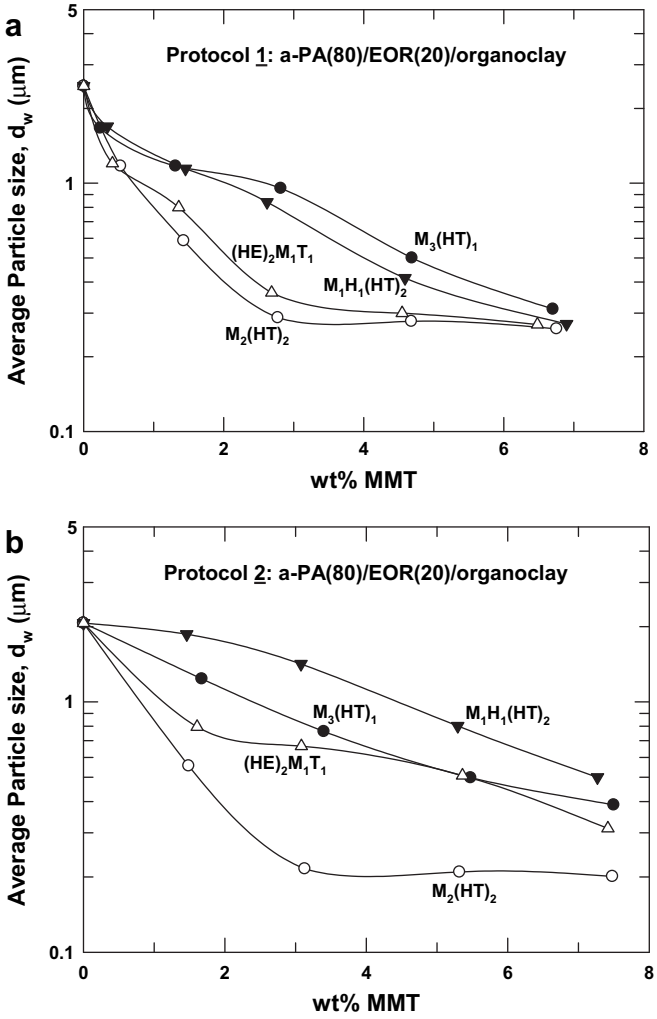

Fig. 6. Effect of organoclay structure on the weight average elastomer particle sizes of a-PA/EOR (80/20) blends prepared by (a) Protocol 1 and (b) Protocol 2, using the indicated organoclays.

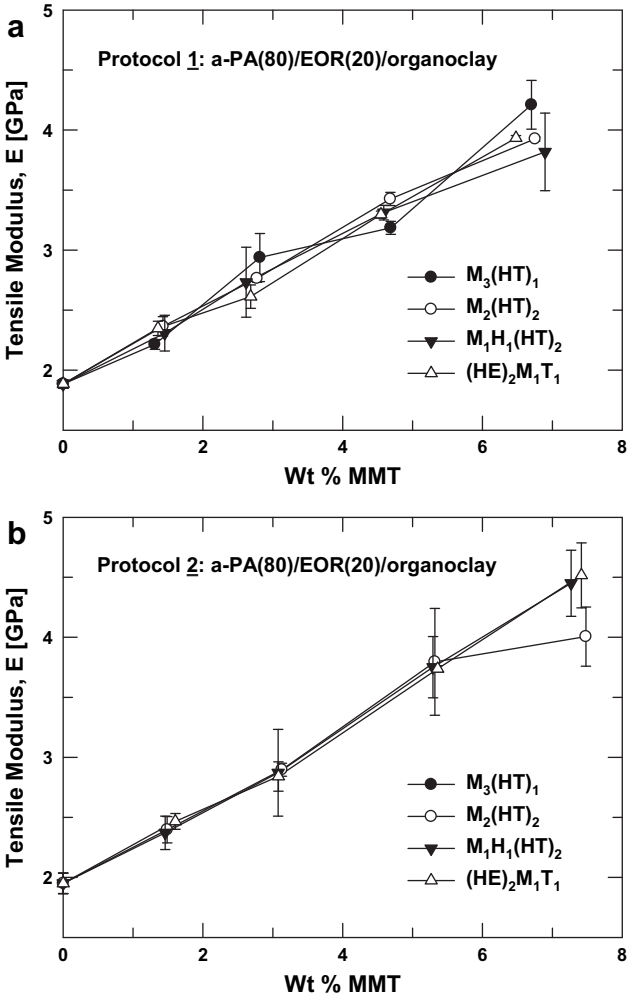

Fig. 7. Effect of organoclay structure on tensile modulus of a-PA/EOR (80/20) blends prepared by (a) Protocol 1 and (b) Protocol 2.

[1]. Measurement of bulk properties such as mechanical, thermal and dynamic mechanical properties complement TEM and WAXS analyses [4,46]. Organoclay structure and mixing protocol do not appear to lead to any substantial differences in the X-ray scattering results in the present cases.

Figs. 4 and 5 show representative TEM micrographs plus histograms that illustrate how elastomer particle morphology depends on the type of organoclay and the mixing protocol. These views are made parallel to the TD of the injection molded bar; the a-PA phase was stained and appears dark while comparatively unstained elastomer particles appear bright. It is clearly observed that elastomer particles are well aligned along the flow direction. Figs, 4(a) and 5(a) show a-PA/EOR blends without any organoclay prepared by the two different mixing protocols. As can be seen, the elastomer particles from both protocols are similarly very large. Interestingly, the elastomer particles do not adhere well to the matrix as shown in Fig. 4(a) and 5(a). However, when 2.8 wt% of MMT is added to the blend prepared by protocol 1, the elastomer particles are well dispersed in the a-PA matrix with dramatically reduced size and irregular shape especially for $M_3(HT)_1$ and $M_2(HT)_2$ as shown in Fig. 4(b) and (c). For the blend prepared by protocol 2 with 3.1 wt% MMT, $M_2(HT)_2$ shows the smallest elastomer particles compared to the nanocomposites from other organoclay as seen in Fig. 5(c). These apparent changes in the morphology of the elastomer phase, e.g., decreasing size and increasing elongated shape as MMT is added, may stem from two competing effects during melt processing; one is rheological in origin while the other stems from the 'barrier' effect of the MMT particles on elastomer particle coalescence [1,4,6,12,15,19–21]. It would appear that the inhibition of coalescence is the more dominant mechanism for reducing elastomer particle size.

Elastomer particle analysis from TEM micrographs can be used to quantify the elastomer particle sizes and size distribution using methods introduced in prior papers [1,2,4,6,32,33]. However, particle analysis for the elastomer phase in a-PA/EOR based nanocomposites is quite complex due to the nonspherical nature of the particles as shown in the TEM micrographs. To determine the size of the elastomer particles, the software used identifies each individual elastomer particle and evaluates its area, A, from which an apparent elastomer particle size, d, was calculated as follows

$$d = \left(\frac{4A}{\pi}\right)^{1/2} \tag{1}$$

A series of histograms of apparent elastomer particle sizes defined by Eq. (1), see Figs. 4 and 5, were built for a-PA/EOR nanocomposites. From the distribution of elastomer particles sizes shown in the histograms, the weight averages of the apparent particle size, $\bar{d}_w$, are calculated as follows [30,47]:

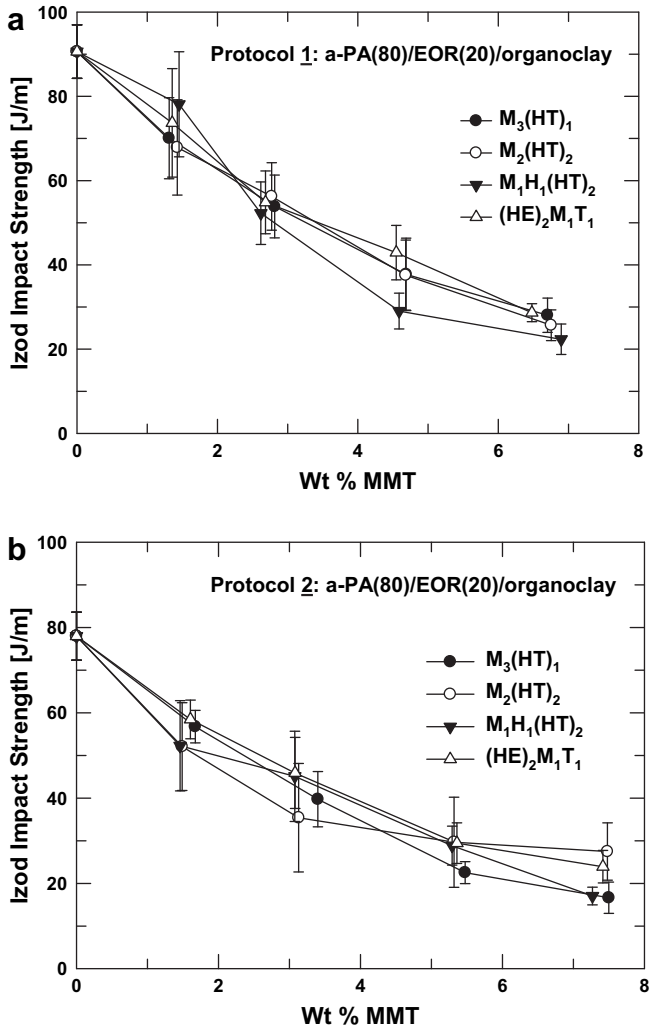

Fig. 8. Effect of organoclay structure on the Izod impact strength of a-PA/EOR (80/20) blends by (a) Protocol 1 and (b) Protocol 2.

$$\bar{d}_w = \frac{\sum n_i d_i^2}{\sum n_i d_i} \tag{2}$$

where n_i is the number of elastomer particles within a specified range about the value d_i. No attempt was made to convert apparent particle sizes into true particle sizes due to the complex nature of the particle shape. Fig. 6 shows the weight average apparent elastomer particle sizes of the nanocomposites, prepared from the two different processing protocols 1 and 2, as a function of MMT content measured from TEM micrographs viewed parallel to TD. The weight average elastomer particle size prepared from two different processing protocols 1 and 2 without organoclay is 2.5 and 2.1 μm, respectively. a-PA/EOR blends prepared from protocol 1 show two typical trends; those from $M_3(HT)_1$ and $M_1H_1(HT)_2$ show a gradual decrease in elastomer particle size over the entire range of MMT contents while for $M_2(HT)_2$ and $(HE)_2M_1T_1$ the decrease in size is more severe with low levels of MMT addition and then more gradual with further increase in MMT content, see Fig. 6(a). On the other hand, blends prepared by protocol 2 with and without the MMT show quite different behavior. Nanocomposites from $M_2(HT)_2$ show a rapid reduction of elastomer particle size with MMT content up to about 3.1 wt% while those from other organoclays, $M_3(HT)_1$, $M_1H_1(HT)_2$ and $(HE)_2M_1T_1$, show a relatively gradual decrease in particle size over the range of MMT content shown in Fig. 6(b). The

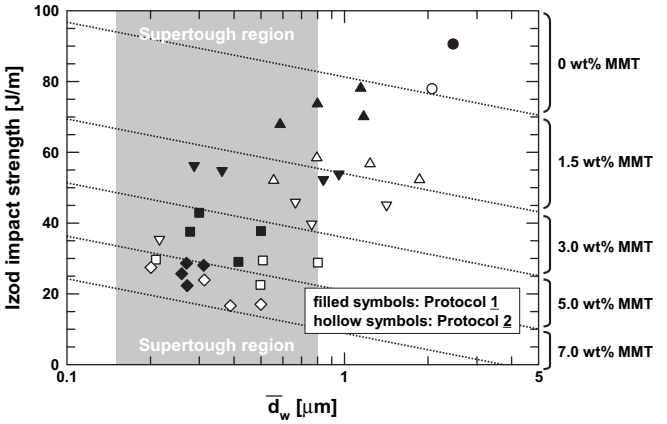

Fig. 9. Effect of average elastomer particle sizes on the Izod impact strength of a-PA/EOR (80/20) blends. The shadowed part refers to the 'supertough region' [31].

largest reduction is observed for the $M_2(HT)_2$ organoclay using protocol 2; the elastomer particle size decreases from 2.1 μm to 0.22 μm in this case. Fig. 6 also compares the effect of the two processing protocols on the elastomer particle size as organoclays are added. In case of protocol 2, considerable difference was observed for blends prepared from 3.1 wt% of MMT based on the versus tertiary amine $M_1H_1(HT)_2$ and the quaternary amine $M_2(HT)_2$ surfactants. However, this difference was not observed in nanocomposites prepared by protocol 1. Broadly speaking, no specific trend or effect of mixing protocols was found. The two preparation protocols used here are similar in that both use two twin-screw extrusion steps and the final compositions are the same.

4. Mechanical properties

Fig. 7 shows the effect of organoclay type and mixing protocol on the tensile modulus of blends of a-PA containing 20 wt% EOR. For both protocols 1 and 2, there is a substantial increase in stiffness over the entire range of MMT contents. In a previous paper, we reported on the effect of organoclay structure on morphology and properties of nanocomposites based on a-PA without any EOR and demonstrated clear differences according to organoclay type; nanocomposites based on the one-tailed organoclay and the organoclay with hydroxyl ethyl groups exhibited exfoliated structures and high matrix reinforcement while nanocomposites from two-tailed organoclay contain a considerable concentration of intercalated stacks and less reinforcement. For blends containing EOR, however, all organoclays lead to similar morphology in a-PA/EOR blends irrespective of surfactant type owing to the two similar preparation protocols as mentioned above. As a result, these organoclays lead to similar trends in mechanical properties of the blend as seen in Fig. 7. In the case of a-PA/EOR blends prepared by protocol 2, the nanocomposite based on $M_2(HT)_2$ exhibits relatively less stiffness enhancement compared to those from $M_3(HT)_1$, $M_1H_1(HT)_2$ and $(HE)_2M_1T_1$. This is similar to results for a-PA nanocomposites based on $M_2(HT)_2$ described previously; the presence of a population of intercalated structures caused the low levels of reinforcement [9].

Fig. 8 shows the influence of the type of organoclay and mixing protocol on the notched Izod impact strength of nanocomposites prepared from a-PA containing 20 wt% EOR at room temperature. All blends prepared by either protocol fail in a brittle matter. No significant trend of the Izod impact strength is seen with the type of organoclay or the mixing protocol. Fig. 9 shows the Izod impact strength of a-PA/EOR blends with different MMT contents versus elastomer particle size. Since no substantial difference was found

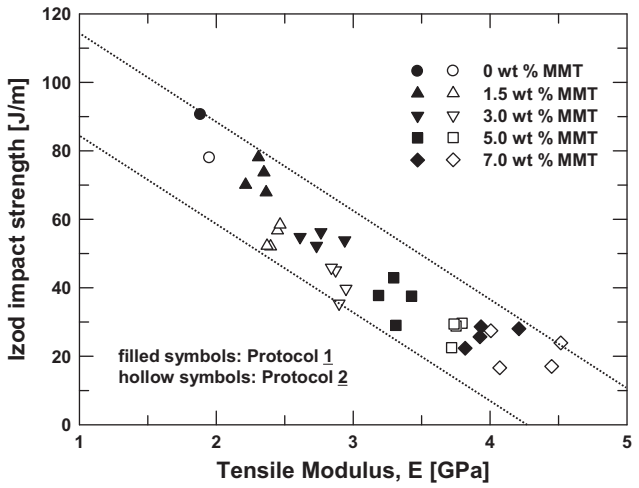

Fig. 10. Relationship between impact strength and tensile modulus of a-PA/EOR (80/20) blends containing organoclays.

according to organoclay type, the structure is not differentiated here. For a-PA/EOR blends based on a maleated version of the elastomer, there is an optimum elastomer particle size, within the range of 0.15–0.8 μm as observed earlier [31], that leads to supertoughness; this region is shown as the shaded area in Fig. 9. For the a-PA/EOR blend without organoclay and with 1.5 wt% MMT, the elastomer particle size is outside the optimum particle size in most cases, and a toughening effect is not expected. For a-PA/EOR blends with higher MMT contents, the elastomer particle size moves within the range where significant toughening would be expected (see shadowed 'supertough region' in Fig. 9 defined from Huang et al. [31].); however, these blends do not exhibit improved toughness. In fact, the toughness decreases as the elastomer particles become smaller by addition of MMT. While addition of MMT increases the stress levels in mechanical tests as shown in Fig. 7, it also reduces the extent of plastic deformation resulting in decreased impact strength. A detailed discussion about this effect can be found in previous reports [2,6,48]. In fact, the toughening response is a complex process where yield strength, viscoelastic behavior, and other matrix effects in addition to blend morphology all play some role [31].

To obtain an overview of the results and the trade-offs involved, Fig. 10 shows the relationship between the Izod impact strength and tensile modulus for a-PA/EOR blends and trade-off as observed in most nanocomposite systems [2,6,8,9,49]. Generally, there is a decrease in ductility as modulus increases due to reinforcement. There is no substantial difference among the organoclay types and the mixing protocols used.

Fig. 11(a) shows Izod impact strength as a function of temperature for a-PA/EOR blends containing 20 wt% EOR and various amounts of $M_3(HT)_1$ prepared by protocol 2; blends based on the other organoclays and mixing protocol were not significantly different. In the absence of MMT, the a-PA/EOR blend starts to show a ductile region above 95 °C but is brittle below 95 °C. Addition of MMT particles increases the ductile–brittle transition temperature (T_{db}) and makes this blend more brittle below this transition; these materials are very brittle and exhibit complete breakage of the specimen during the impact test as shown in Fig. 11(b). In fact, the T_{db} for these nanocomposites was not observed within the experimental range. Interestingly, while all samples failed in a brittle manner at low Izod values, some samples exhibit hinged breaks.

Fig. 12 shows the effect of elastomer and MMT content on the impact strength of blend nanocomposites based on $M_3(HT)_1$

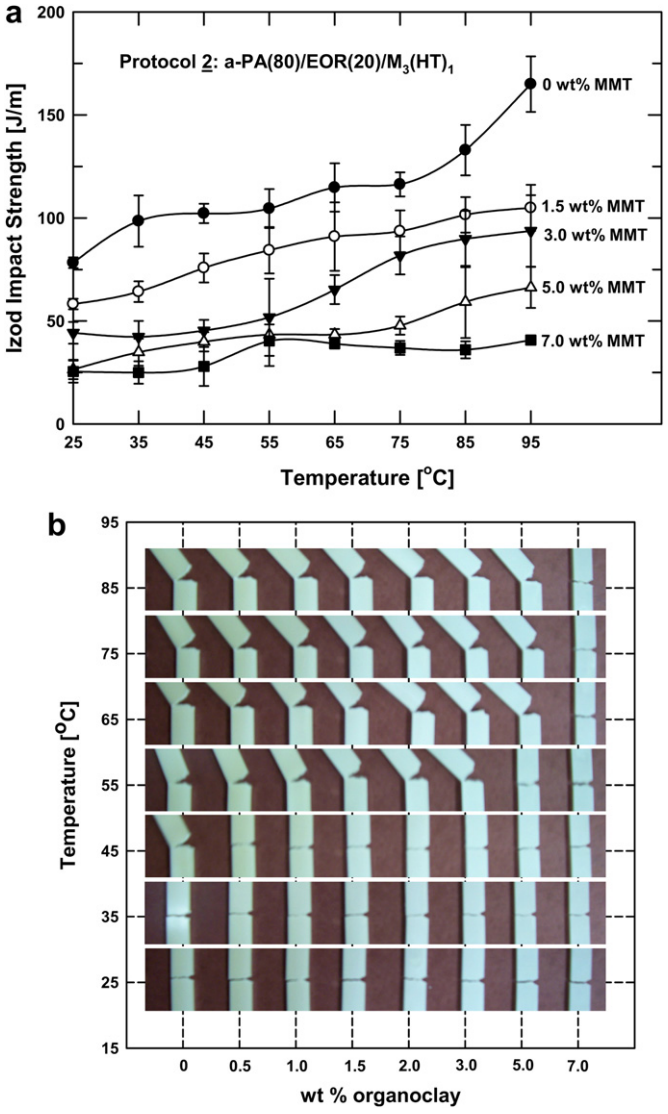

Fig. 11. (a) Effect of organoclay content on the impact strength of a-PA/EOR (80/20) blends prepared from $M_3(HT)_1$ using Protocol 1 (b) Photographs of Izod specimens taken after the notched impact test for the same materials.

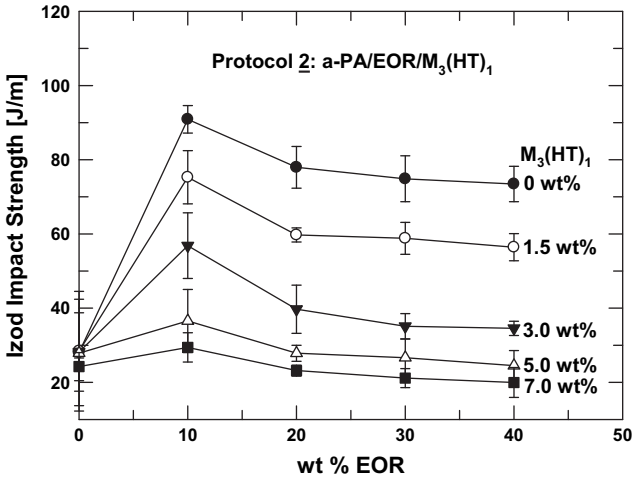

Fig. 12. Effect of elastomer and organoclay contents on the Izod impact strength of a-PA/EOR (80/20) blends prepared from $M_3(HT)_1$ using Protocol 1.

prepared by protocol 2. There is an increase in impact strength with elastomer content up to 10 wt%, but beyond this, elastomer content has no significant effect on impact strength. While the addition of MMT reduces elastomer particle size to an extent where supertoughness could be expected, it does not provide any improvement in impact strength. Increasing the MMT content decreases impact strength irrespective of elastomer content in the nanocomposite. The impact strength decreases rapidly up to 3 wt% MMT with less significant change beyond this. The mechanical constraint imposed by MMT particles in a-PA dominates the effect MMT has on elastomer morphology leading to brittle behavior for ternary nanocomposites. This trend is opposite to that observed by Lee at al. [1], for PP/elastomer nanocomposites. These authors reported brittle to ductile transition for TPO nanocomposites at high elastomer content (~30 and 40 wt%). The MMT content required to achieve supertoughness decreased as the elastomer content increased from 30 to 40 wt%. The reason for the vast differences in toughening response between the polyamide versus polypropylene systems is not currently known at this time but is actively being investigated as part of other studies in our laboratory.

5. Conclusions

In this study, the possibility of toughening a-PA with an EOR elastomer was examined using organoclays to control the elastomer phase morphology. Two different mixing protocols and four different organoclays, $M_3(HT)_1$, $M_2(HT)_2$, $M_1H_1(HT)_2$ and $(HE)_2M_1T_1$, were used to explore the effect of the organoclay structure and the mixing protocol on the morphology and properties of these blends. Detailed morphological studies for the dispersed clay and elastomer and subsequent quantitative particle analyses for the elastomer phases revealed that most of the organoclay is well exfoliated in the a-PA phase, but some of the organoclay locates at the interface and tends to envelop the EOR phase. The apparent size of the elastomer particles initially decreased rapidly with organoclay content but the rate of reduction decreased at higher loadings. The presence of organoclay causes the elastomer particles to become elongated and irregular in shape. No significant effect of mixing protocol or organoclay type on the final morphology was observed although small differences in size and shape of the elastomer particles were seen. The smallest elastomer particles were produced using the organoclay based on $M_2(HT)_2$ in blends prepared by protocol 2. The trends of mechanical properties for these nanocomposite blends appear to be broadly the same irrespective of the mixing protocol and the organoclay type; the tensile modulus is enhanced by increasing the organoclay content whereas the impact strength decreases in a clear trade-off relationship.

Acknowledgements

This work was supported in part by a grant from General Motors Global Research and Development; the authors would like to thank William R. Rodgers for his continued interest. The authors sincerely thank Dr. P. J. Yoon and Dr. D. L. Hunter of Southern Clay Products, Inc. for providing organoclay materials and many helpful discussions and Mr. Tony Gonzalez for his help with WAXS analyses. We also thank Du Pont and ExxonMobil for providing the polymers used in this work.

References

[1] Lee H-S, Fasulo PD, Rodgers WR, Paul DR. Polymer 2005;46(25):11673–89.
[2] Ahn Y-C, Paul DR. Polymer 2006;47(8):2830–8.
[3] Lee H-S, Fasulo PD, Rodgers WR, Paul DR. Polymer 2006;47(10):3528–39.
[4] Kim DH, Fasulo PD, Rodgers WR, Paul DR. Polymer 2007;48(20):5960–78.
[5] Kim DH, Fasulo PD, Rodgers WR, Paul DR. Polymer 2008;49(10):2492–506.
[6] Yoo Y, Cui L, Yoon PJ, Paul DR. Macromolecules 2010;43(2):615–24.
[7] Fornes TD, Hunter DL, Paul DR. Macromolecules 2004;37(5):1793–8.
[8] Fornes TD, Yoon PJ, Hunter DL, Keskkula H, Paul DR. Polymer 2002;43 (22):5915–33.
[9] Yoo Y, Paul DR. Polymer 2008;49:3795–804.
[10] Dharaiya DP, Jana SC. J Polym Sci Part B Polym Phys 2005;43(24):3638–51.
[11] Gahleitner M, Kretzschmar B, Vliet GV, Devaux J, Pospiech D, Bernreitner K, et al. Rheol Acta 2006;45(4):322–30.
[12] Gelfer MY, Song HH, Liu L, Hsiao BS, Chu B, Rafailovich M, et al. J Polym Sci Part B Polym Phys 2003;41(1):44–54.
[13] Gersappe D. Phys Rev Lett 2002;89(5):058301-1–058301-4.
[14] Hong JS, Namkung H, Ahn KH, Lee SJ, Kim C. Polymer 2006;47(11):3967–75.
[15] Khatua BB, Lee DJ, Kim HY, Kim JK. Macromolecules 2004;37(7):2454–9.
[16] Ray SS, Bousmina M. Polymer 2005;46(26):12033–738.
[17] Si M, Araki T, Ade H, Kilcoyne ALD, Fisher R, Sokolov JC, et al. Macromolecules 2006;39(14):4793–801.
[18] Vo LT, Giannelis EP. Macromolecules 2007;40(23):8271–6.
[19] Voulgaris D, Petridis D. Polymer 2002;43(8):2213–8.
[20] Wang Y, Zhang Q, Fu Q. Macromol Rapid Commun 2003;24(3):231–5.
[21] Yoo Y, Park C, Lee S-G, Choi K-Y, Kim DS, Lee JH. Macromol Chem Phys 2005;206(8):878–84.
[22] González I, Eguiazábal JI, Nazábal J. J Polym Sci Part B Polym Phys 2005;43 (24):3611–20.
[23] González I, Eguiazábal JI, Nazábal J. Eur Polym J 2006;42(11):2905–13.
[24] Lee MH, Dan CH, Kim JH, Cha J, Kim S, Hwang Y, et al. Polymer 2006;47 (12):4359–69.
[25] Kelnar I, Khunova V, Kotek J, Kapralkova L. Polymer 2007;48(18):5332–9.
[26] Dasari A, Yu Z-Z, Mai Y-W. Polymer 2005;46(16):5986–91.
[27] García-López D, López-Quintana S, Gobernado-Mitre I, Merino JC, Pastor JM. Polym Eng Sci 2007;47(7):1033–9.
[28] Ha MH, Kim MS, Kim BK, Kim W, Lee MC, Kim HD. J Appl Polym Sci 2004;92 (2):804–11.
[29] Wang K, Wang C, Li J, Su J, Zhang Q, Du R, et al. Polymer 2007;48(7):2144–54.
[30] Huang JJ, Keskkula H, Paul DR. Polymer 2004;45(12):4203–15.
[31] Huang JJ, Keskkula H, Paul DR. Polymer 2006;47(2):639–51.
[32] Huang JJ, Keskkula H, Paul DR. Polymer 2006;47(2):624–38.
[33] Oshinski AJ, Keskkula H, Paul DR. Polymer 1996;37(22):4891–907.
[34] Cui L, Bara JE, Brun Y, Yoo Y, Yoon PJ, Paul DR. Polymer 2009;50 (11):2492–502.
[35] Yoon PJ, Fornes TD, Paul DR. Polymer 2002;43(25):6727–41.
[36] Stretz HA, Paul DR. Polymer 2006;47(24):8123–36.
[37] Oshinski AJ, Keskkula H, Paul DR. Polymer 1996;37(22):4919–28.
[38] Fornes TD, Yoon PJ, Keskkula H, Paul DR. Polymer 2001;42(25):9929–40.
[39] Stretz HA, Paul DR. Polymer 2006;47(26):8527–35.
[40] Stretz HA, Paul DR, Li R, Keskkula H, Cassidy PE. Polymer 2005;46 (8):2621–37.
[41] Fornes TD, Paul DR. Macromolecules 2004;37(20):7698–709.
[42] Shah RK, Paul DR. Polymer 2004;45:2991–3000.
[43] Pickering SU. J Chem Soc 1907;91:2001–21.
[44] Aveyard R, Binks BP, Clint JH. Adv Colloid Interface Sci 2003;100-102:503–46.
[45] Dennis HR, Hunter DL, Chang D, Kim S, White JL, Cho JW, et al. Polymer 2001;42(23):9513–22.
[46] Kim DH, Fasulo PD, Rodgers WR, Paul DR. Polymer 2007;48(18):5308–23.
[47] Irani RR, Callis CF. Particle size: measurement, interpretation, and application. New York: Wiley; 1963.
[48] Bucknall CB, Paul DR. Polymer 2009;50(23):5539–48.
[49] Yoon PJ, Hunter DL, Paul DR. Polymer 2003;44(18):5323–39.
[50] Xanthos M, Parmer JF, Forest MLL, Smith GR. J Appl Polym Sci 1996;62 (8):1167–77.
[51] Ellis TS. Macromolecules 1991;24(13):3845–52.